

Military Technical College
Kobry Elkobbah,
Cairo, Egypt



8th International Conference
on Aerospace Sciences &
Aviation Technology

MODELING PENETRATION OF CERAMIC/METAL LIGHTWEIGHT ARMOURS BY SMALL AND MEDIUM CALIBER PROJECTILES

A. M. RIAD*

ABSTRACT

In this paper, an analytical model is developed to describe the penetration of ceramic/metal lightweight armours by small and medium caliber projectiles, respectively. Both the projectile and back plate materials are assumed to behave as rigid-perfectly plastic with respect to their nominal stress-engineering strain relationships. Two modes are associated with the back plate and the projectile, respectively, during the penetration process; these are erosion and rigid. The model identifies three main phases for the penetration of a lightweight armour; these are: (i) ceramic fragmentation, (ii) penetration of fragmented ceramic and (iii) penetration of back plate. Phase (i) consists mainly of one stage, whereas the other two, i.e. phase (ii) and phase (iii), consist mainly of different penetration stages, respectively. The current penetration stage is ascertained according to the relative velocities between the projectile mass and the mass of remaining ceramic and/or the mass of the back plate ahead of projectile. The main equations representing each penetration stage are derived based on momentum conservation principle.

The present model is capable of predicting the time-histories of the velocities of the moving masses and the projectile penetration depth through ceramic/metal lightweight armour as well as post-perforation results. Matching predicted results of the present model with the experimental and numerical results of other investigators serves to determine the flow stress of the ceramic material globally. The present results are concerned with design optimization of ceramic/metal lightweight armours capable of defeating small and medium caliber projectiles. The influence of ceramic thickness and strength as well as back plate thickness and strength on the ballistic limit of the armours considered is presented and discussed. Moreover, the effect of ceramic thickness on projectile remaining mass and residual velocity are discussed.

KEY WORDS

- Dynamics
- Solid Mechanics
- Impact Dynamics
- Penetration Mechanics

* Lecturer, Chair of Weapons and Ammunition, M.T.C., Cairo, Egypt.

INTRODUCTION

Armour design is important to develop more efficient protection systems against the threat of modern kinetic energy projectiles. Traditionally, armours have been made monolithic, usually of high strength steel. Although rolled armour steel is still, and will continue to be, the most widely used material, the demands of achieving lightweight armours led to the investigation of alternate materials. Such materials are needed to improve the ballistic protection as well as to reduce the weight of existing armours. In the last three decades, other materials, such as ceramics and composites, have been incorporated into more efficient lightweight armours.

Investigating the penetration process through a lightweight armour is necessary for design optimization of such an armour. Three main research directions are used for studying the penetration of a lightweight armour by small and medium caliber projectiles. These directions are: (i) experimental, (ii) numerical simulation and (iii) analytical ones. Experimental work could lead to useful empirical relations, e.g. relations between ballistic limit and areal density, respectively, due to the normal impact of ceramic/metal targets by small caliber projectiles and those due to oblique impact of such targets by such projectiles [1]. These relations are hardly extrapolated to configurations other than those tested. Determination of ballistic efficiency of ceramic by measuring the depth of penetration into back plate and comparing it with its counterpart into metallic targets can also be tackled [2,3]. Selecting the most efficient combination of armour components to provide the lightest protection system of ceramic/FRP against any perceived level of threat is another objective of experimentation [4].

Numerical simulations are based on integrating the differential equations of the mechanics of continuum media using finite difference codes such as AUTODYN or finite elements codes such as LS-DYNA and HEMP. Such work requires a large number of sets of data of materials involved and some parametric approximations, while its predictive capacity is limited. Numerical work can simulate the impact process of an Armour Piercing Discarding Sabot, APDS, projectile into ceramic/steel and ceramic/FRP armours and determine penetrator length after penetration, residual velocity and pressure below ceramic [5]. Designing lightweight armours consisting of ceramic/metal and ceramic/composite has also been performed numerically, e.g. [6].

Analytical work is the fastest, less expensive, and probably most accurate research direction in this field. It is based on introducing simplified assumptions to derive the projectile equations of motion. It also simulates the impact process in a few seconds using personal computers. Examples of analytical work include: (a) deriving the ballistic limit equations for ceramic/FRP target [4] as well as ceramic/metal target [7], (b) modeling the penetration of ceramic backed by metal [8] and ceramic backed by fabric [9] based on momentum balance to determine the optimal thickness of various components, (c) specifying the penetration of

ceramic backed by metal using a three-stage model based on equating the pressure at the projectile/target interface [10,11], and (d) optimization of ceramic/composite armours via determination of ballistic limit as function of areal density and ceramic thickness [12].

In the following, an analytical model is developed to describe the penetration of a ceramic/metal target by small and medium caliber projectiles, respectively. In this model, both the projectile and back plate materials are assumed to behave as rigid-perfectly plastic with respect to their nominal stress-engineering strain relationships and the model identifies two modes associated with them during the penetration process; these are erosion and rigid. The model consists of three main phases; these are: (i) ceramic fragmentation, (ii) penetration of fragmented ceramic and (iii) penetration of back plate. The main features associated with the target penetration are identified (ceramic erosion, ceramic conoid formation, erosion and penetration of back plate). The governing equations of each penetration phase are derived based on momentum conservation principle.

The main equations representing the different phases of the model are compiled into a computer program. The input data to the program are easily determined. Comparison of current predicted results with experimental and numerical results of other investigators leads to the determination of the global value of the ceramic flow stress. Samples of predicted ceramic/metal lightweight armours capable of defeating small and medium caliber projectiles, respectively, are presented; optimization of such armours is also conducted. The influence of thickness and strength of both ceramic tile and back plate materials, respectively, on the ballistic resistance of ceramic/metal lightweight armours are presented and discussed. The effect of ceramic thickness on the residual mass and velocity of projectile after perforation are also discussed.

ANALYTICAL MODEL

In this model, the projectile is idealized as a cylindrical rod of initial length L_0 and initial diameter D_0 . Similar to the one-dimensional analytical models developed by Tate [13,14] and Alekseevskii [15], the projectile material is assumed to behave as rigid-perfectly plastic with respect to its nominal stress-engineering strain relationship. Therefore, the present model identifies two modes associated with the penetrating projectile through the target; these modes are erosion and rigid. The projectile is assumed to strike the target normally with a high-speed velocity.

The present model considers the lightweight armour to consist of a ceramic tile of thickness H_c , backed by a metallic plate of thickness H_b . As mentioned before, the model divides the penetration process of the ceramic/metal lightweight armour by a high-speed projectile into three main phases. These phases are: (i) ceramic fragmentation, (ii) penetration of fragmented ceramic and (iii) penetration of back plate phases. The phase (i) consists mainly of one stage whereas the other two penetration phases consist mainly of different penetration stages, respectively.

The back plate material is assumed to behave as rigid-perfectly plastic with respect to its nominal stress-engineering strain relationship and it may be eroded or moves as a rigid mass during penetration.

The model is based on equating the interface force at the rod-target interface. The momentum conservation principle is used to derive the main equations representing each penetration stage. The sequence of penetration stages depends on the relative velocities between projectile mass and mass of the remaining fragmented ceramic and/or mass of the back plate ahead of projectile. The different sequences of penetration stages that represent the complete penetration process of a ceramic/metal lightweight armour by a high-speed projectile are shown in Fig. 1.

For each penetration stage, a system of first order dependent differential equations has been derived. This system is solved numerically. The penetration time is taken to be the independent variable. The end conditions of the current penetration stage are considered as the initial conditions for the subsequent stage. The system solution gives the velocity of the rod, the penetration velocity and the velocities of the ceramic mass and the back plate mass ahead of projectile, the projectile penetration depth, the bulge height and the interface force as functions of the penetration time. The penetration process terminates when the projectile front reaches the backface of the back plate or when the projectile stops inside the armour, i.e. it attains zero velocity.

In the following, the physical concepts considered and the main assumptions adopted for modeling the penetration of a ceramic/metal lightweight armour by a high-speed projectile are presented. The main equations representing each penetration stage of each phase are derived; these equations are listed in Table 1.

Physical Concepts and Main Assumptions

Ceramic fragmentation phase (cf. Fig. 2a):

- When the rod impacts the ceramic tile, a crack initiates at the backface of ceramic tile and propagates fast compared with the projectile velocity to the front of the penetrating projectile.
- The crack forms a cone of fractured ceramic and it separates the loaded region inside the cone from an unloaded region outside the cone.
- The diameter of fractured cone is assumed to be equal to the rod diameter plus four times the thickness of ceramic tile [7]. Experimentation gives a cone angle of 68° [1].
- Both the front of rod and surface of ceramic tile are eroded; erosion means a physical separation of material. Therefore, the momentum of eroded materials for rod and ceramic, respectively, do not contribute to ceramic penetration.

- According to the estimated velocity profile, the rod penetrates the ceramic with penetration velocity U , whereas the remaining ceramic inside the cone and back plate are assumed to be stationary.
- The ceramic flow stress is assumed to be constant during this phase and is denoted by Y_{c_0} .

Penetration of fragmented ceramic phase (cf. Fig. 2b):

- The penetration process through the fragmented ceramic cone is assumed to be localized. Therefore, the ceramic material of fractured cone ahead of the penetrating projectile as well as the localized mass of the back plate contribute to the target penetration.
- The localized masses of ceramic and back plate ahead of projectile are accelerated forward with an estimated velocity profile allowing for compatibility with the moving projectile.
- The eroded zone for the rod and ceramic has a velocity U , whereas the remaining fragmented ceramic and back plate masses ahead of projectile move with a velocity W . Moreover, a bulge starts to protrude from the backface of the back plate; it has a height h .
- The projectile mode may be changed from erosion to rigid during this phase. This change occurs when the velocity of the rigid part of the projectile V is equal to the penetration velocity U .
- The ceramic may be fully eroded or subject to erosion. The erosion terminates when the remaining mass of fragmented ceramic ahead of projectile moves with a velocity equal to the penetration velocity U . The ceramic flow stress decreases due to its fragmentation and is denoted by Y_c .
- The motion of fragmented ceramic and back plate material ahead of projectile is resisted by the shear force due to the ultimate shear strength of back plate material which acts on the periphery of the moving back plate mass.

Penetration of back plate phase (cf. Figs. (2)c and (2)d):

- The projectile alone or the projectile and remaining mass of fragmented ceramic penetrate the back plate; the projectile mode may change from erosion to rigid.
- When the ceramic is fully eroded, the back plate surface ahead of projectile may be subject to erosion. The erosion terminates when this back plate mass attains a velocity equal to the current penetration velocity U . Bulge continues to protrude from the backface of the plate.
- The shear force is the only force that resists the motion of the moving masses; it decreases with the increase of projectile penetration depth through the back plate.
- The transfer of projectile penetration from ceramic to back plate gives a non-uniform distribution of the penetration velocity.
- This stage terminates when the projectile stops inside the back plate or reaches the backface of the back plate which fails by plugging.

Table 1. Main equations representing each phase of the developed Model.

<p>I- The following equation holds for the three phases:</p> <p>* Time rate of change of projectile penetration depth Z:</p> $dZ/dt = U, \tag{1}$ <p>U: current penetration velocity.</p>	
<p>II- For eroding projectile, the following equations hold for the three phases:</p> <p>* Time rate of change of length of projectile rigid part:</p> $dL/dt = - (V-U), \tag{2}$ <p>L: length of projectile rigid part, V: current velocity of projectile rigid part.</p>	
<p>* Deceleration of projectile rigid part during penetration:</p> $dV/dt = - Y_p / (\rho_p L), \tag{3}$ <p>Y_p: flow stress of projectile material, ρ_p: density of projectile material.</p>	
<p>III- The following equation holds for phases (ii) and (iii):</p> <p>* Time rate of change of bulge height:</p> $dh/dt = W, \tag{4}$ <p>h: bulge height, W: current velocity of remaining fragmented ceramic and back plate materials ahead of projectile during phase (ii) and/or phase (iii), or velocity of back plate material ahead of projectile during phase (iii).</p>	
<p>IV- Phase (i): ceramic fragmentation (cf. Fig. 2a):</p> <p>* Force at projectile-ceramic interface, F_i [8]:</p> $F_i = Y_p A_o + \rho_p A_o V(V-U) = Y_{c_r} A_o + \rho_c A_o U^2, \tag{5}$ <p>A_o: cross-sectional area of projectile, Y_{c_r}: flow stress of ceramic, ρ_c: density of ceramic.</p>	
<p>* Current penetration velocity U as a function of velocity of projectile rigid part V:</p> $U = (-V + [(1+4\mu) V^2 - A]^0.5) / 2\mu, \tag{6}$ <p>where $\mu = \rho_c / \rho_p$, $\tag{6a}$</p> <p>and $A = 4\mu (Y_{c_o} - Y_p) / \rho_p$. $\tag{6b}$</p>	
<p>* End condition:</p> $Z + S_{crack} = H_{c_o}, \tag{7}$ <p>where $S_{crack} = V_{crack} \cdot t$, $\tag{7a}$</p> <p>S_{crack}: distance traveled by the crack front through ceramic thickness, H_{c_o}: initial thickness of ceramic, and V_{crack}: velocity of crack propagation through ceramic which equals to one-fifth the value of longitudinal velocity of stress wave through ceramic material [10]. t: penetration time.</p>	

Table 1. Main equations representing each phase of the developed Model (continued).

<p>V- Phase (ii): Penetration of fragmented ceramic: Stage (1): Penetration of eroding projectile into fragmented ceramic, (V > U, U > W, Z < Hc_o), (cf. Fig. 2b):</p>	
<p>* Force at projectile-ceramic interface, F₁ :</p>	$F_1 = Y_p A_o + \rho_p A_o V(V-U) = Y_c A_o + \rho_c A_o U(U-W), \quad (8)$
<p>Y_c: flow stress of fragmented ceramic.</p>	
<p>* Current flow stress of fragmented ceramic given by [10]:</p>	$Y_c = Y_{c_o} [(V-W)/V_{s_1}]^2, \quad (9)$
<p>V_{s₁} : velocity of projectile rigid part when ceramic fragmentation phase terminates.</p>	
<p>* Current penetration velocity U as function of V and W:</p>	$U = \frac{- (V - \mu W) + [(V - \mu W)^2 + 4\mu (V^2 - (Y_c - Y_p) / \rho_p)]^{0.5}}{2\mu}. \quad (10)$
<p>* Time rate of change of fragmented ceramic thickness:</p>	$dH_c/dt = -(U-W), \quad (11)$
<p>H_c: current thickness of fragmented ceramic.</p>	
<p>* Acceleration of masses of remaining fragmented ceramic and back plate ahead of projectile:</p>	$dW/dt = (Y_c A_o - F_s)/M_t, \quad (12)$
<p>where</p>	$F_s = \pi D_o \tau H_b, \quad (12a)$
<p>and</p>	$M_t = \rho_B A_o H_b + \rho_c A_o H_c, \quad (12b)$
<p>F_s : shear force, M_t : mass of remaining fragmented ceramic and back plate ahead of projectile, D_o : projectile diameter, τ : ultimate shear strength of back plate material, H_b : initial thickness of back plate, ρ_B : density of back plate material.</p>	
<p>* End conditions:</p>	$Z = H_{c_o}, V = U \text{ or } U = W. \quad (13)$
<p>Stage (2): Eroding projectile penetration into remaining fragmented ceramic, (V > U, U = W, Z < Hc_o):</p>	
<p>* Force at projectile-ceramic interface, F₁ :</p>	$F_1 = Y_p A_o + \rho_p A_o V(V-U) = Y_c A_o, \quad (14)$
<p>Y_c: current flow stress of fragmented ceramic: it is calculated by Eqn. (9).</p>	
<p>* Acceleration of remaining fragmented ceramic and back plate masses ahead of projectile:</p>	

Table 1. Main equations representing each phase of the developed Model (continued).

$dW/dt = ((Y_p + \rho_p V(V-U)) A_o - F_s)/M_t \quad (15)$	
* End condition:	$V = U \quad (16)$
<p>Stage (3): Rigid projectile penetration into fragmented ceramic, $(V = U, U > W, Z < Hc_o)$:</p>	
* Force at projectile-ceramic interface, F_i :	$F_i = Y_p A_o = Y_c A_o + \rho_c A_o U(U-W), \quad (17)$
<p>Y_c is calculated by Eqn. (9).</p>	
* Deceleration of projectile during penetration:	$dV/dt = - ((Y_c + \rho_c U(U-W)) A_o) / \rho_p L_r, \quad (18)$
<p>L_r: length of rigid part of projectile when its erosion terminates.</p>	
* In addition to Eqn. (11).	
* End condition:	$Z = Hc_o \text{ or } U = W. \quad (19)$
<p>VI- Phase (iii): Projectile penetration into back plate:</p>	
<p>Stage (1): Back plate penetration by eroding projectile, $(V > U, U > W)$, (cf. Fig. 2c):</p>	
* Force at projectile-back plate interface, F_i :	$F_i = Y_p A_o + \rho_p A_o V(V-U) = Y_B A_o + \rho_B A_o U(U-W), \quad (20)$
<p>Y_B: constrained dynamic yield strength of back plate material [16], ρ_B: density of back plate material.</p>	
* Penetration velocity U as function of V and W :	$U = \frac{- (V - \mu_B W) + [(V - \mu_B W)^2 + 4\mu_B (V^2 - (Y_B - Y_p) / \rho_p)]^{0.5}}{2\mu_B}, \quad (21)$
where	$\mu_B = \rho_B / \rho_p. \quad (21)a$
* Time rate of change of back plate thickness:	$dH_{bc}/dt = -(U-W), \quad (22)$
<p>H_{bc}: current thickness of back plate.</p>	
* Acceleration of rigid part of moving mass from the back plate:	$dW/dt = (Y_B A_o - F_{sc})/M_B, \quad (23)$
where	$F_{sc} = \pi D_o \tau (H_b + Hc_o + h - Z), \quad (23)a$

Table 1. Main equations representing each phase of the developed Model (continued).

and	$M_B = \rho_B A_o H_{bc}$	(23)b
* End condition:	$V = U$ or $U = W$.	(24)
Stage (2): Eroding projectile penetration into back plate, ($V > U$, $U = W$):		
* Force at projectile-back plate interface, F_i :	$F_i = Y_p A_o + \rho_p A_o V(V-U) = Y_B A_o$	(25)
* Acceleration of rigid mass of back plate ahead of projectile:	$dU/dt = ((Y_p + \rho_p V(V-U)) A_o - F_{sc})/M_B$	(26)
* End condition:	$V = U$.	(27)
Stage (3): Rigid projectile penetration into back plate, ($V = U$, $U > W$):		
* Force at projectile-back plate interface, F_i :	$F_i = Y_p A_o = Y_B A_o + \rho_B A_o U(U-W)$	(28)
* Deceleration of projectile during penetration:	$dV/dt = -((Y_B + \rho_B U(U-W)) A_o) / \rho_B L_r$	(29)
* In addition to Eqns. (22) and (23).		
* End condition:	$U = W$.	(30)
Stage (4): Rigid projectile penetration into back plate (continued), ($V = U = W$):		
* Deceleration of moving projectile-plug masses:	$(\rho_p A_o L + \rho_B A_o H_{bc}) dV/dt = -F_{sc}$	(31)
* In addition to Eqn. (23)a.		
* End condition:	$Z = H_{c_o} + H_b$	(32)
Stage (5): Penetration of rigid projectile and remaining ceramic into back plate, ($V = U = W$), (cf. Fig. 2d):		
* Deceleration of moving masses:	$(\rho_p A_o L + \rho_c A_o H_c + \rho_B A_o H_{bc}) dV/dt = -F_{sc}$	(33)
* In addition to Eqn. (23)a.		
* End condition: Eqn. (32).		

RESULTS AND DISCUSSIONS

In the following, results of the developed model are classified into: (i) model validation and (ii) predictions which include: (a) design optimization of lightweight armour, (b) post-perforation results concerned with determination of the projectile residual velocity and its mass after perforation and (c) influence of armour parameters on its ballistic resistance.

(i) Validation of the Developed Model

* For small caliber projectiles

To validate the present model for small caliber projectiles, the experimental results obtained by Wilkins have been used [6]. Wilkins determines the ballistic limits for ceramic/aluminium targets impacted by 7.62 mm armour piercing projectiles. The tested lightweight targets consisted of AD85 ceramic tiles backed by 6061-T6 aluminium alloy plates.

The program is run to predict the ballistic limits of ceramic/aluminium targets that were tested by Wilkins. The input data to the computer program for the materials of projectile and ceramic/aluminium targets, respectively, are listed in Table 2. The dynamic yield strength of projectile and back plate materials, respectively, are determined following the procedure of Ref. [17]. The flow stress of projectile material, Y_p , is equal to its dynamic yield strength, whereas the flow stress of back plate material, Y_B , is equal to its dynamic yield strength multiplied by a constrained factor; the value of this factor is 2.7 [16]. The ceramic flow stress is represented initially by its yield strength.

The predicted ballistic limits of the ceramic/aluminium targets and the corresponding experimental values obtained by Wilkins are listed in Table 3. The predicted results are generally lower than the corresponding experimental values. Woodward [8] fit the experimental data of Wilkins with the predicted results of his model to determine the flow stress of AD85 ceramic. He recommended that: (i) the flow stress of ceramic could be represented by its hardness divided by a factor; this factor varies from 1 to 2.9, (ii) the flow stress of ceramic increases with its thickness. In the following, the matching of the predicted results of the present model with the experimental results of Wilkins determines the global value of flow stress for AD85 ceramic; this value is considered to be constant for the different thicknesses of ceramic tiles.

The predicted ballistic limits for the different ceramic/aluminium targets using the determined value of ceramic flow stress are listed in Table 3. The differences between the predicted ballistic limits and the corresponding experimental values of Wilkins are also listed in Table 3. Good agreement is generally obtained between predicted ballistic limits and experimental values of Wilkins when the determined value of ceramic flow stress is considered (i.e. $Y_{c_0} = 5.2$ GPa). In

Table 2. Input data to the computer program.

Parameter	Proj. caliber, D _o [mm]		Ceramic tiles			Aluminium alloy		
	7.62	25	AD85	Al-N	AD85.4	6061-T6	7075-T6	6063-T5
- projectile flow stress, Y _p [GPa]	2.35	2.35						
- penetrator mass, [g]	5.46	95						
- initial flow stress, Y _{c0} [GPa]			3.8	6.7	5.7			
- used flow stress, Y _{c0} [GPa]			5.2	8.0	6.2			
- Young's modulus, E _c [GPa]			267	300	350			
- density, ρ _c [g/cm ³]			3.43	3.42	3.84			
- dynamic yield strength, [MPa]						372	588	333
- flow stress, Y _B [GPa]						1.05	1.587	0.9
- density, ρ _B [g/cm ³]						2.75	2.75	2.75
- strain to fracture, ε _f [%]						17	11	9.0

Table 3. Experimental [6] and predicted ballistic limits of AD85 ceramic/6061-T6 Al alloy armours impacted by 7.62 mm projectiles.

Ceramic thickness H _{c0} [mm]	Aluminium thickness H _b [mm]	Measured ballistic limit [6], [m/s]	Predicted ballistic limits V _{BL} [m/s]		Relative difference [%]
			Y _{c0} = 3.8 GPa	Y _{c0} = 5.2 GPa	
5.8	7.24	735	606	724	-1.5
7.83	7.24	894	668	788	-11.8
5.8	6.35	701	582	702	-
7.83	6.35	847	645	767	-9.4
6.35	5.08	623	556	684	9.8
	6.35	703	599	719	2.8
	7.62	752	633	751	-
	8.89	789	664	774	-1.9
	9.5	818	681	780	-4.6
7.85	4.35	643	568	702	9.2
	5.76	705	630	752	6.7
	7.64	821	679	798	-2.8
	9.3	901	720	829	-8.0

addition, the maximum relative difference between the predicted ballistic limit and the corresponding experimental value of Wilkins was found to be 11.8%.

*** For medium caliber projectiles**

The developed model is also validated for medium caliber projectiles, the numerical results of Zaera et al. have been used [10]. They simulate the impact of a 25 mm APDS projectile into ceramic/aluminium targets using AUTODYN-2D hydrocode. Their targets consisted of Al-N ceramic tile backed by 7075-T6 aluminium alloy plate and AD99.5 ceramic tile backed also by 7075-T6 aluminium alloy plate, respectively. The input data to the computer program for the materials of projectile and ceramic/aluminum targets are listed in Table 2. The global values of flow stress for Al-N and AD99.5 ceramic tiles are determined by matching the predicted results of the model with the corresponding numerical results of Zaera et al. The predicted values of flow stress are 8 GPa for Al-N ceramic and 6.2 GPa for AD99.5 ceramic. In addition, these values are not changed with the ceramic thickness.

Figure 3 plots the predicted change of projectile residual velocity with aluminium alloy thickness for the different values of flow stress of Al-N ceramic. In addition, the corresponding numerical results of Zaera et al. are also depicted on the same figure. The 25 mm projectile impacts normally the target that consists of equal thickness of Al-N ceramic tile and 7075-T6 aluminium alloy plate with a velocity of 1275 m/s. Good agreement is generally obtained between predicted results of the present model and numerical results of Zaera et al. when the flow stress of ceramic is 8.0 GPa. Moreover, the program predicts that a target thickness of 83 mm (41.5 mm thick Al-N ceramic + 41.5 mm thick 7075-T6 aluminium alloy) is capable of defeating such a projectile, whereas a corresponding target thickness of 84 mm (42 mm thick Al-N ceramic + 42 mm thick 7075-T6 aluminium alloy) is predicted by numerical results of Zaera et al.

Figure 4 also depicts the predicted change of projectile residual velocity with AD99.5 ceramic thickness for the different values of flow stress of such a ceramic. The corresponding numerical results of Zaera et al. are also depicted on the same figure. The targets consist of AD99.5 ceramic tiles backed by 7075-T6 aluminium alloy plates. The ceramic thickness is changed, whereas a 35 mm thick aluminium alloy plate is used for backing the ceramic tiles. It is clear from the figure that the predicted results of the present model are in good agreement with the numerical results of Zaera et al. when the considered flow stress of ceramic is equal to 6.2 GPa. In addition, the model predicts that a target thickness of 93 mm (58 mm thick AD99.5 ceramic + 35 mm thick 7075-T6 aluminium alloy) is capable of defeating such a projectile, whereas a corresponding target thickness of 88 mm (53 mm thick AD99.5 ceramic + 35 mm thick 7075-T6 aluminium alloy) is predicted by numerical results of Zaera et al.

The flow stress of ceramic is considered to be constant with ceramic thickness. The predicted results of the developed model could be made better when the ceramic flow stress is taken to be proportional to the ceramic thickness. In addition, a few tests are needed to determine the flow stress of ceramic for further application of the present model to investigate the penetration process of other lightweight armours.

(ii) Predictions

Design optimization of lightweight armour

In the following, a 7.62 mm armour piercing projectile is considered to impact a lightweight armour consisting of an AD85 ceramic tile backed by a 5083-H3 aluminium alloy plate and a 25 mm APDS projectile impacting into an armour consisting of an AD99.5 ceramic tile backed by a plate having the same class of aluminium alloy. The 7.62 mm projectile is assumed to impact the armour with three velocities ranging from 750 to 850 m/s with an increment of 50 m/s, whereas the 25 mm projectile impacts its corresponding armour with another three velocities ranging from 1000 to 1200 with an increment of 100 m/s. The input data to the computer program for the projectiles, ceramics and backing plates listed in Table 2 are fed into the program.

For a 7.62 mm AP projectile, Fig. 5 depicts the predicted change of AD85 ceramic thickness with 5083-H3 aluminium alloy thickness at different impact velocities. For each impact velocity, the program predicts a group of armour thicknesses, addition of ceramic thickness and corresponding aluminium alloy thickness, capable of defeating the projectile. Similarly for a 25 mm APDS projectile, Fig. 6 plots the predicted change of AD99.5 ceramic thickness with 5083-H3 aluminium alloy thickness at different impact velocities. The trends are similar to those shown in Fig. 5 and the program also predicts a group of armour thicknesses capable of defeating such a projectile at each impact velocity. Therefore, it is necessary to have another factor determining the optimum design of armour at each impact velocity.

Because of the importance of the weight of the armour, the areal density is taken as a measure of armour weight when the optimum design is needed. Figure 7 depicts the change of areal density of armour capable of defeating a 7.62 mm projectile with 5083-H3 aluminium alloy thickness at different impact velocities. Moreover, Fig. 8 plots similar trends of the change of areal density of armour capable of defeating a 25 mm APDS projectile with the corresponding 5083-H3 aluminium alloy thickness at different impact velocities. At each impact velocity, the optimum design of the armour corresponds to the minimum areal density. For a 7.62 mm projectile having an impact velocity of 850 m/s, the optimum design of armour constitutes a 10.3 mm thick AD85 ceramic tile backed by a 7 mm thick 5083-H3 aluminium alloy plate; this armour has an areal density of 54.4 kg/m². For a 25 mm APDS projectile having an impact velocity of 1200 m/s, the optimum design of armour constitutes a 58.3 mm thick AD99.5 ceramic tile backed by a 24 mm thick 5083-H3 aluminium alloy plate; such an armour has an areal density of 289.4 kg/m².

Post-perforation results

In the following, the influence of armour thickness on the residual velocity and mass of projectile is presented. For a 7.62 mm projectile, Fig. 9 depicts the change of projectile residual mass ratio, M_r/M_0 , with ceramic thickness and the

change of projectile residual velocity ratio, V_r/V_i , with the total armour thickness at $V_i = 900$ m/s. The considered armours consist of AD85 ceramic tiles of different thicknesses backed by 8 mm thick 5083-H3 aluminium alloy plate. It is clear from the figure that both the projectile residual velocity ratio and the projectile residual mass ratio decrease with the increase of ceramic thickness. This is attributed to the increase of time during which the projectile is subjected to erosion with ceramic thickness. In addition, the energy necessary for defeating the armour increases with armour thickness. The model predicts that the projectile lost 33% of its velocity and 18.7% of its mass in defeating an armour having a total thickness of 12 mm. In addition, the projectile lost 93% of its velocity and 34.8% of its mass in defeating an armor having a total thickness of 19 mm.

For a 25 mm projectile having $V_i = 1200$ m/s, Fig. 10 plots the change of projectile residual mass ratio with ceramic thickness and the change of projectile residual velocity ratio with the total armour thickness. The considered armours consist of AD99.5 ceramic tiles of different thicknesses backed by 30 mm thick 5083-H3 aluminium alloy plate. Similar trends to those shown in Fig. 9 for the projectile residual velocity ratio and its residual mass ratio with ceramic thickness are obtained. In addition, the model predicts that the projectile lost 27% of its velocity and 31.9% of its mass in defeating an armor having a total thickness of 50 mm, whereas the projectile lost 48% of its velocity and 42.4% of its mass in defeating an armour having a total thickness of 66 mm.

Effect of armour parameters on its ballistic resistance

In the following, the ballistic limit is the factor used to evaluate the influence of armour parameters on its ballistic resistance.

*** Effect of thickness and strength of ceramic**

In the following, two classes of ceramic are considered; these are AD85 and AD99.5. Each ceramic tile of the two different classes is backed by a 5083-H3 aluminium alloy plate. For a 7.62 mm projectile, the thickness of ceramic tile of each class is changed while the back plate is assumed to have a thickness of 8 mm. The input data of projectile, ceramic and back plate listed in Table 2 are fed into the program.

Figure 11 depicts the change of ballistic limit of the considered lightweight armours with ceramic thickness for the two classes of ceramic. It is clear from the figure that the ballistic limit of armour increases with ceramic thickness. For the same ceramic thickness, the ballistic limit of armour also increases with the strength of ceramic. For $V_i = 865$ m/s, the model predicts that the total armour thickness defeating the 7.62 mm projectile decreases by 16.7% and its weight decreases by 13.2% if the AD85 ceramic is replaced by AD99.5 ceramic.

For a 25 mm APDS projectile, the same constitutions of lightweight armours considered with the 7.62 mm projectile are considered. In addition, 30 mm thick 5083-H3 aluminium alloy plates back the ceramic tiles of different classes, respectively. Figure 12 plots the change of ballistic limit of the considered

armours with ceramic thickness for the two classes of ceramic. Similar trends for the change of ballistic limit with ceramic thickness to those shown in Fig. 11 are obtained. For $V_1 = 870$ m/s, the model predicts that the total armour thickness defeating such a projectile decreases by 13.3% and its weight decreases by 10% if the AD85 ceramic is replaced by AD99.5 ceramic.

*** Effect of thickness and strength of back plate material**

In the following, two classes of aluminium alloys are considered; these are 7075-T6 and 5083-H3. For a 7.62 mm projectile, the facing material of the considered armour is AD85 ceramic having a thickness of 8 mm. The input data for projectile, ceramic and the two aluminium alloy classes listed in Table 2 are fed into the program.

Figure 13 depicts the change of ballistic limit of the considered armours with aluminium alloy thickness for the two classes of aluminium alloy. It is clear from this figure that the ballistic resistance of armour increases with back plate thickness. In addition, the ballistic resistance of armour increases with the strength of back plate material. For $V_1 = 850$ m/s, the model predicts that the total armour thickness defeating the 7.62 mm projectile decreases by 9.1% and its weight also decreases by 4.8% if the 5083-H3 aluminium alloy back plate is replaced by 7075-T6 aluminium alloy plate.

For a 25 mm APDS projectile, Fig. 14 depicts the change of ballistic limit of armours consisting of a 20 mm thick AD99.5 ceramic tiles backed by 5083-H3 and 7075-T6 aluminium alloy plates, respectively, with aluminium alloy thickness. Similar trends to those shown in Fig. 13 are obtained. For $V_1 = 850$ m/s, the model predicts that the total thickness of armour decreases by 10% and its weight by 5.1% if the 5083-H3 aluminium alloy plate is replaced by 7075-T6 aluminium alloy plate.

CONCLUSIONS

An analytical model describing the penetration process due to the impact of small and medium caliber projectiles into ceramic/aluminium armours has been developed. The model consists of three main phases; these are: (i) ceramic fragmentation, (ii) penetration of fragmented ceramic and (iii) penetration of back plate. The first phase consists of only one penetration stage, whereas the other two phases include a group of penetration stages, respectively. The sequence of penetration stages depends on the relations between the velocity of the rigid part of the projectile, the penetration velocity and the velocity of ceramic and/or back plate material ahead of projectile.

The governing equations of each penetration stage are derived and compiled into a computer program. Matching predicted residual velocities of projectile and ballistic limits with the numerical and experimental results of other investigators serves to determine the flow stress of ceramics. The results presented are

concerned with: (i) design optimization of ceramic/Al alloy lightweight armours capable of defeating the 7.62 mm AP and 25 mm APDS projectiles, (ii) studying the effect of armour thickness on residual velocity and mass of such projectiles and (iii) studying the effects of thickness and strength of ceramic and back plate materials, respectively, on the ballistic resistance of armour. For further application of the model to investigate the penetration of lightweight armour by a high-speed projectile, a few tests could be performed on such armours. The test results serve to determine ceramic flow stress. Moreover, the ceramic flow stress may be considered to vary with ceramic thickness.

REFERENCES

1. Sadanandan, S. and Hetherington, J., "Characterization of Ceramic/Steel and Ceramic/Aluminium Armours Subjected to Oblique Impact", *Int. J. Impact Engng.*, Vol. 19, pp. 811-819 (1997).
2. Yaziv, D. and Partom, Y., "The Ballistic Efficiency of Thick Alumina Targets Against Long Rod Penetrators", 16th Int. Symp. on Ballistics, Quebec, Canada, 26-29 September (1993).
3. Rosenberg Z. and Yeshurun, Y., "The Relation Between Ballistic Efficiency and Compressive Strength of Ceramic Tiles", *Int. J. Impact Engng.*, Vol. 7, No. 3, pp. 357-362 (1988).
4. Hetherington, J. and Rajagopalan, B., "An Investigation Into the Energy Absorbed During Ballistic Perforation of Composite Armours", *Int. J. Impact Engng.*, Vol. 11, No. 1, pp. 33-40 (1991).
5. Thoma, K., Buffel, P., Deisenroth, U. and Wieland, W., "Penetration of An APDS Projectile Into a Ceramic Layered Target-Experimental Results and Their Interpretation by Calculation", 16th Int. Symp. on Ballistics, Quebec, Canada, 26-29 September (1993).
6. Wilkins, M. L., "Third Progress Report of Light Armour Program", Lawrence Radiation Laboratory, University of California, U.S.A., UCRL-50460, July (1968).
7. Florence, A. L., "Interaction of Projectiles and Composite Armours", Part II, Stanford Research Institute, Menlo Park, California, U.S.A., AMMRG-CR-69-15, August (1969).
8. Woodward, R. L., "A Simple One-Dimensional Approach to Modeling Ceramic Composite Armour Defeat", *Int. J. Impact Engng.*, Vol. 9, No. 4, pp. 455-474 (1990).
9. Walker, J. D. and Anderson, Jr., C. E., "An Analytical Model for a Ceramic Tile, Substrate and Fabric", 17th Int. Symp. on Ballistics, Midrand, South Africa, March 23-27 (1998).
10. Zaera, R., Galvez, F., Rodriguez J. and Sanchez-Galvez, V., "Design of Ceramic-Metal Armours Against Medium Caliber Projectiles", 17th Int. Symp. on Ballistics, Midrand, South Africa, March 23-27 (1998).

11. Zaera R. and Sanchez-Galvez, V., "Analytical Modeling of Normal and Oblique Ballistic Impact on Ceramic/Metal Lightweight Armour", *Int. J. Impact Engng.*, Vol. 21, No. 3, pp. 133-148 (1998).
12. Chocron, S., Galvez, V. S., Rubio, F. G., Walker J. D. and Anderson, Jr., C. E., "Analytical Study and Optimization of Ceramic/Composite Armour to a Range of Projectile Threats", 17th Int. Symp. on Ballistics, Midrand, South Africa, March 23-27 (1998).
13. Tate, A., "A Theory for the Deceleration of Long Rods After Impact", *J. Mech. Phys. Solids*, Vol. 15, pp. 387-399 (1967).
14. Tate, A., "Further Results in the Theory of Long Rod Penetration", *J. Mech. Phys. Solids*, Vol. 17, pp. 141-150 (1969).
15. Alekseevskii, P., "Penetration of a Rod Into a Target at High Velocity" *Combustion, Explosion and Shock waves*, No. 2, pp. 63-66 (1966).
16. Woodward R. L. and De Morton, M. E., "Penetration of Targets by Flat Ended Projectiles", *Int. J. Mech. Sci.*, Vol. 18, pp. 119-127 (1976).
17. Recht, R. F., "Taylor Ballistic Impact Modeling Applied to Deformation and Mass Loss Determination", *Int. J. Engng. Sci.*, Vol. 16, pp. 809-827 (1978).

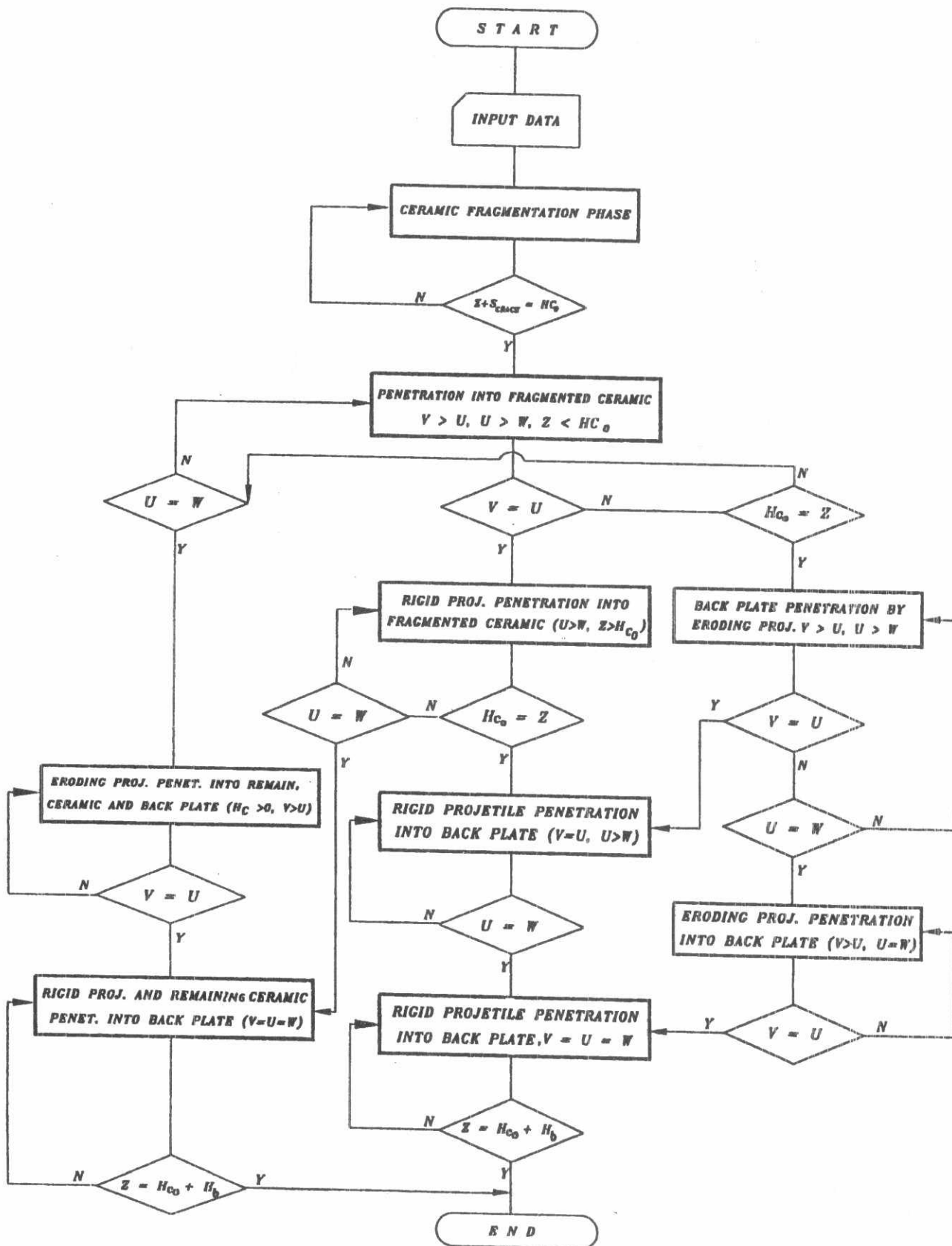


Fig. 1. Flow chart showing the different penetration stages representing the complete penetration process of a ceramic/metal armour by a projectile.

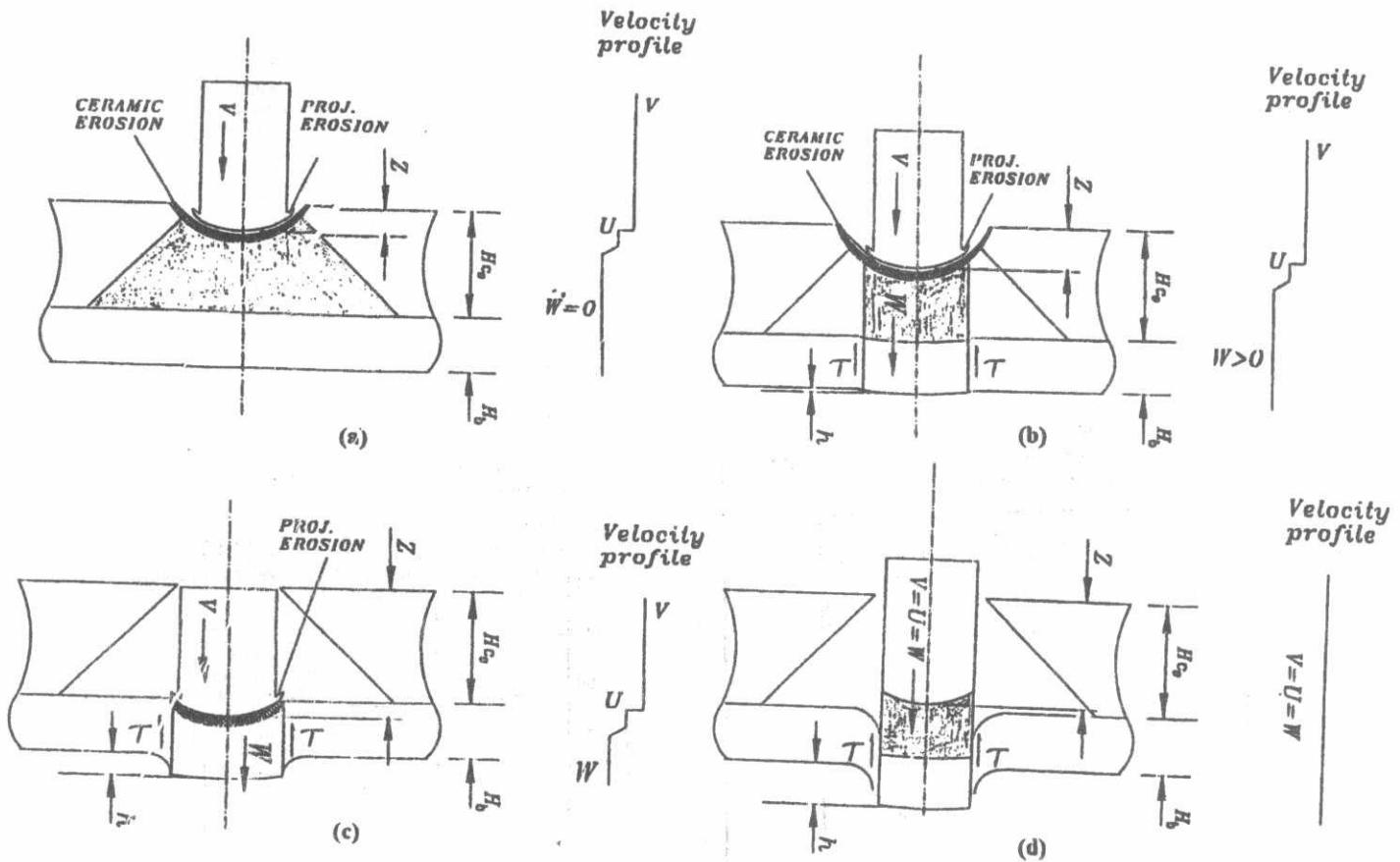


Fig. 2. Diagrammatic scheme of some penetration stages and their estimated velocity profiles; these are: (a) ceramic fragmentation, (b) penetration into fragmented ceramic ($V > U, U > W, Z < H_{c_0}$), (c) penetration of eroding projectile into back plate ($V > U, U > W$) and (d) penetration of rigid projectile and remaining ceramic into back plate ($V = U = W$).

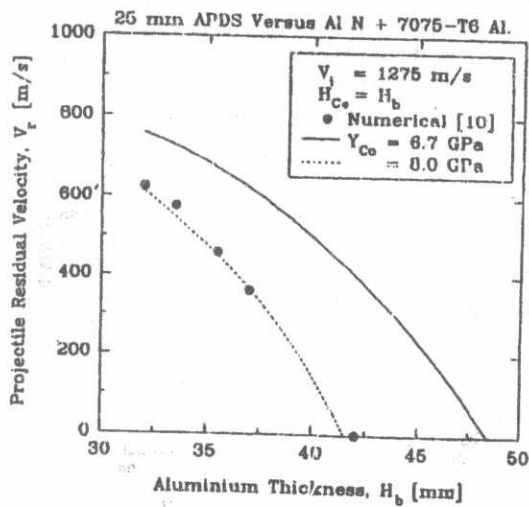


Fig. 3. Numerical [10] and predicted projectile residual velocity versus Al. alloy thickness for different values of ceramic flow stress due to the impact of 25 mm projectile into Al-N ceramic/7075-T6 Al. alloy armours.

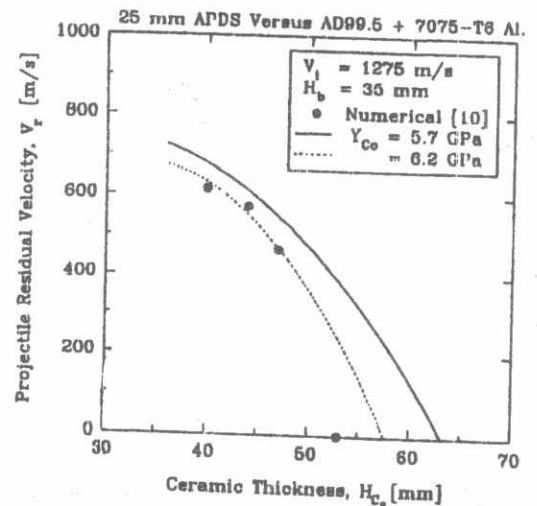


Fig. 4. Numerical [10] and predicted projectile residual velocity versus ceramic thickness for different values of ceramic flow stress due to the impact of 25 mm projectile into AD99.5 ceramic/7075-T6 Al. alloy armours.

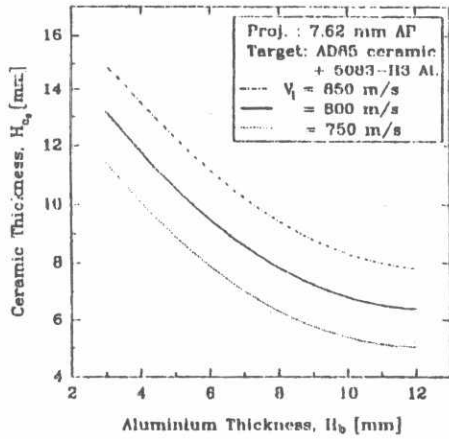


Fig. 5. Predicted AD85 ceramic thickness and corresponding 5083-H3 Al. alloy thickness capable of defeating a 7.62 mm AP projectile at different impact velocities.

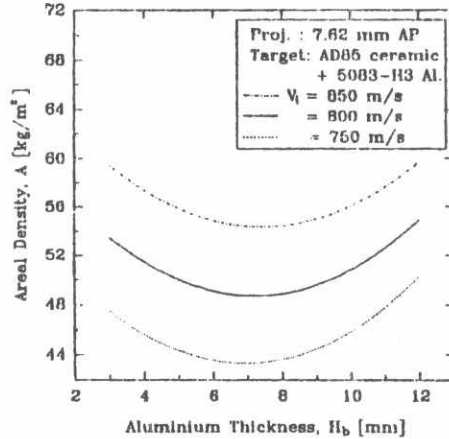


Fig. 7. Predicted change of areal density of armours capable of defeating a 7.62 mm AP projectile with 5083-H3 Al. alloy thickness at different impact velocities.

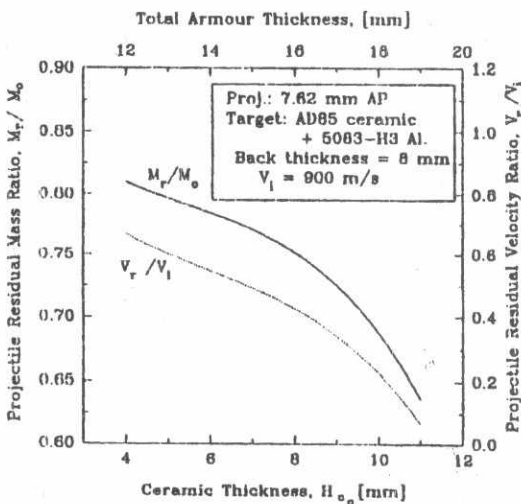


Fig. 9. Predicted change of projectile velocity and mass ratios after the perforation of AD85 ceramic/5083-H3 Al. alloy armour by a 7.62 mm AP projectile with AD85 ceramic thickness.

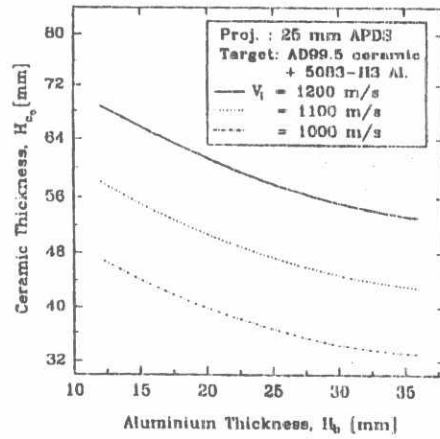


Fig. 6. Predicted AD99.5 ceramic thickness and corresponding 5083-H3 Al. alloy thickness capable of defeating a 25 mm APDS projectile at different impact velocities.

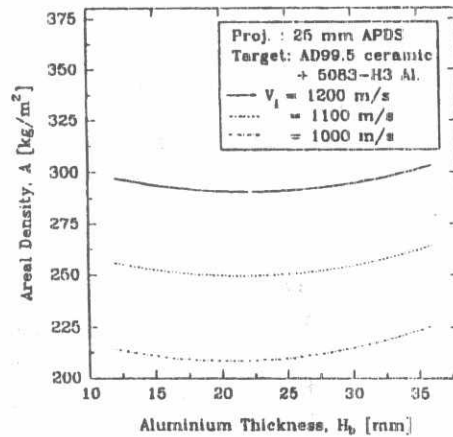


Fig. 8. Predicted change of areal density of armours capable of defeating a 25 mm APDS projectile with 5083-H3 Al. alloy thickness at different impact velocities.

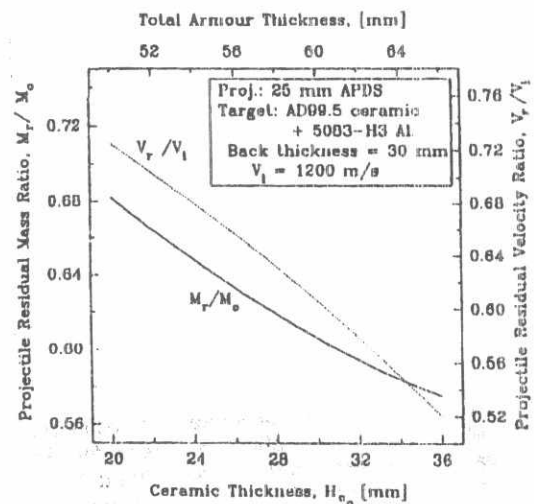


Fig. 10. Predicted change of projectile velocity and mass ratios after the perforation of AD99.5 ceramic/5083-H3 Al. alloy armour by a 25 mm AP DS projectile with AD99.5 ceramic thickness.

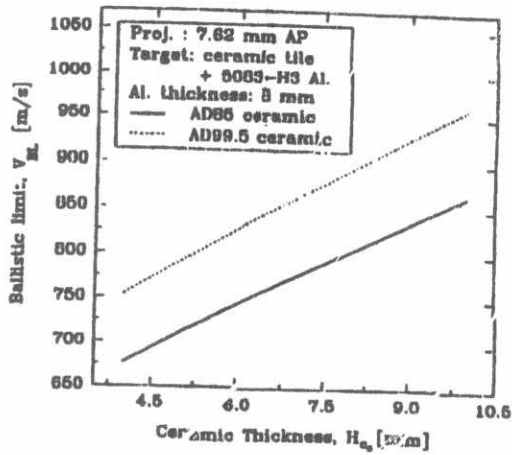


Fig. 11. Predicted ballistic limit of ceramic/5083-H3 Al. alloy armour capable of defeating a 7.62 mm projectile versus ceramic thickness for two ceramic classes.

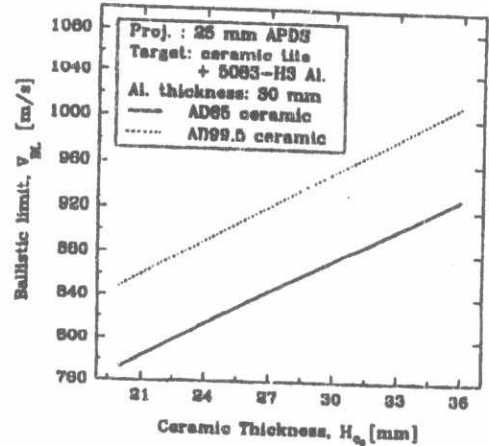


Fig. 12. Predicted ballistic limit of a ceramic/5083-H3 Al. alloy armour capable of defeating a 25 mm projectile versus ceramic thickness for two ceramic classes.

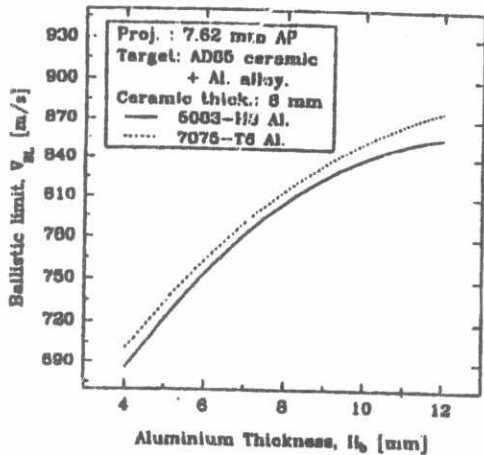


Fig. 13. Predicted ballistic limit of an AD85 ceramic/Al. alloy armour capable of defeating a 7.62 mm projectile versus Al. alloy thickness for two classes of Al. alloy.

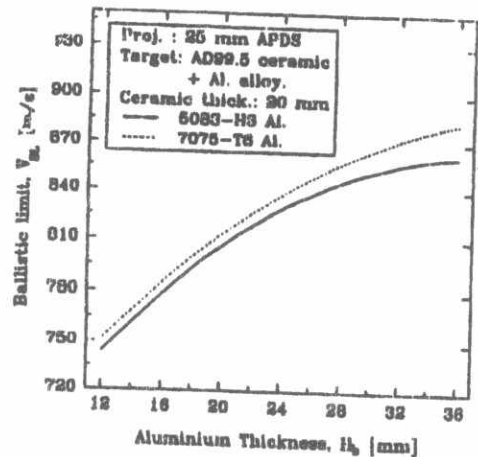


Fig. 14. Predicted ballistic limit of an AD99.5 ceramic/Al. alloy armour capable of defeating a 25 mm projectile versus Al. alloy thickness for two classes of Al. alloy.